Photoswitchable diacylglycerols enable optical control of protein kinase C

James Allen Frank[1], Dmytro A. Yushchenko[2,3], David J. Hodson[4,5,6], Noa Lipstein[7], Jatin Nagpal[8,9], Guy A. Rutter[4], Jeong-Seop Rhee[7], Alexander Gottschalk[8,9], Nils Brose[7], Carsten Schultz*[2], Dirk Trauner*[1]

[1]Department of Chemistry and Center for Integrated Protein Science, Ludwig Maximilians University Munich, Butenandtstraße 5-13, 81377 Munich, Germany. [2]European Molecular Biology Laboratory (EMBL), Cell Biology & Biophysics Unit, Meyerhofstraße 1, 69117 Heidelberg, Germany. [3]Institute of Organic Chemistry and Biochemistry, Academy of Sciences of the Czech Republic, Flemingovo namesti 2, 16610 Prague 6, Czech Republic. [4]Section of Cell Biology and Functional Genomics, Department of Medicine, Imperial College London, ICTEM, Hammersmith Hospital, Du Cane Road, London W12 0NN, UK. [5]Institute of Metabolism and Systems Research (IMSR), University of Birmingham, Birmingham B15 2TT, UK. [6]Centre for Endocrinology, Diabetes and Metabolism, Birmingham Health Partners, Birmingham, B15 2TH, UK. [7]Department of Molecular Neurobiology, Max Planck Institute of Experimental Medicine, Hermann-Rein Straße 3, 37075 Göttingen, Germany. [8]Buchmann Institute for Molecular Life Sciences, Goethe University, Max von Laue Strasse 15, D-60438 Frankfurt, Germany. [9]Institute of Biochemistry, Department for Biochemistry, Chemistry and Pharmacy, Goethe University, Max von Laue Strasse 9, D-60438 Frankfurt, Germany.

ABSTRACT

Increased levels of the second messenger lipid diacylglycerol (DAG) induce downstream signaling events including the translocation of C1 domain-containing proteins toward the plasma membrane. Here, we introduce three light-sensitive DAGs, termed PhoDAGs, which feature a photoswitchable acyl chain. The PhoDAGs are inactive in the dark and promote the translocation of proteins that feature C1 domains towards the plasma membrane upon a flash of UV-A light. This effect is quickly reversed after the termination of photostimulation or by irradiation with blue light, permitting the generation of oscillation patterns. Both protein kinase C and Munc13 can thus be put under optical control. PhoDAGs control vesicle release in excitable cells, such as mouse pancreatic islets and hippocampal neurons, and modulate synaptic transmission in *Caenorhabditis elegans*. As such, the PhoDAGs afford an unprecedented degree of spatiotemporal control, and are broadly applicable tools to study DAG signaling.

INTRODUCTION

Diacylglycerol (DAG) is not only an integral component of plasma membrane phospholipids, but is also known for its role as a second messenger[1]. Cellular DAG concentrations are tightly regulated by enzymes including phospholipase C, as well as DAG lipases and kinases[2]. The bulk of DAG originates from phosphatidylcholine, or the phospholipase C-mediated hydrolysis of phosphoinositides. Rapid changes in DAG levels occur following the extracellular stimulation of receptors[3]. Over 50 different DAGs have been identified in humans[4], and the length and degree of unsaturation of the lipid chains determines the biophysical and pharmacological properties of individual DAG species[5].

DAGs interact with both transmembrane and soluble proteins, and are known to activate Transient Receptor Potential (TRP) cation channels, including TRPC3 and TRPC6[6]. Importantly, DAG generation also triggers the translocation towards the plasma membrane of a number of proteins that contain C1 domains[7]. These small, highly conserved, zinc-binding protein domains were originally characterized as the DAG-sensing regulatory elements of the protein kinase C (PKC) family[8]. C1-mediated translocation plays a key role in the activation of various other factors, including kinases and nucleotide exchange factors[2]. DAGs were also reported to affect the protein machinery involved in synaptic transmission and exocytosis[2,9]. Thus, a tool which enables reversible control of C1 domain translocation would be widely applicable towards the control of intra- and intercellular signaling.

Precision pharmacological manipulation of lipid signaling is often difficult due to the restricted localization and diffusion of these hydrophobic molecules. Experimentally, the activation of C1 domain-containing proteins is usually achieved by addition of bryostatins or phorbol-esters, which can be viewed as highly potent DAG mimics[10]. So far, the greatest control over DAG concentrations has been achieved with the photochemical uncaging of DAGs, such as caged 1,2-*O*-dioctanoyl-*sn*-glycerol (*cg*-1,2-DOG)[11]. However, once triggered, the activity cannot be switched OFF and the decay of the DAG signal depends on its metabolism or diffusion from the cell. Alternatively, chemical dimerizers[12,13] or optogenetic techniques[14] may be employed to modulate the levels of signaling lipids in cells on the addition of a small molecule or a flash of light, respectively. While these systems hold great promise for rapid switching

within signaling networks, they require recombinant expression of non-native proteins, and frequently depend on the presence of exogenous co-factors.

Previously, we prepared a series of photoswitchable fatty acids, termed FAAzos[15], which can mimic highly unsaturated fatty acids such as arachidonic acid. They are useful modular building blocks for synthetic incorporation into more elaborate photolipids. We now report the incorporation of the FAAzos into the DAG scaffold. The resulting photoswitchable DAGs, PhoDAGs, allow us to mimic the effects of natural DAGs in living cells with unprecedented kinetics and reversibility, especially in regards to pattern formation.

RESULTS

Design and synthesis of photoswitchable DAGs

The design of the PhoDAGs was guided by our previous work which suggested that the azobenzene derivative **FAAzo-4** (**Fig. 1a**), in its *cis*-configuration, is able to mimic arachidonic acid[15]. Therefore, we synthesized **PhoDAG-1** (**1**) as a photoswitchable analog of 2-*O*-arachidonyl-1-*O*-stearoyl-*sn*-glycerol (1,2-SAG) (**Fig. 1b**). **PhoDAG-1** was intended to be less active with the azobenzene in the *trans*-form, and become more active upon isomerization to the *cis*-form with UV-A light. The more hydrophilic DAG derivatives, **PhoDAG-2** (**2**) and **PhoDAG-3** (**3**), were designed as cell-permeable analogs mimicking 1,2-*O*-dioctanoyl-*sn*-glycerol (1,2-DOG)[16], and contain shorter alkyl chains at the *sn*1 and *sn*2 positions, including the shorter chain azobenzene **FAAzo-9** (**4**) (**Supplementary Results**, **Supplementary Note 1**).

PhoDAG-1 was synthesized in four steps in 57% overall yield (**Supplementary Note 2a**). When handled under ambient lighting conditions, **PhoDAG-1** existed predominantly in its thermally stable *trans*-configuration and contained approximately 10% *cis*-isomer (**Supplementary Note 2b**). On irradiation with UV-A light (λ = 350–375 nm), **PhoDAG-1** isomerized to its *cis*-configuration (**Fig. 1c**). Thermal back-relaxation of *cis*-**PhoDAG-1** occurred with a τ-value of about 60 h in DMSO and 22 h in water, while blue irradiation increased the rate of isomerization from *cis* to *trans.* As such, **PhoDAG-1** behaves as a regular azobenzene, and can be switched over many cycles without fatigue (**Fig. 1d**). The remaining PhoDAGs were prepared in an analogous fashion (**Supplementary Note 2c**), and possessed comparable spectral characteristics to **PhoDAG-1**.

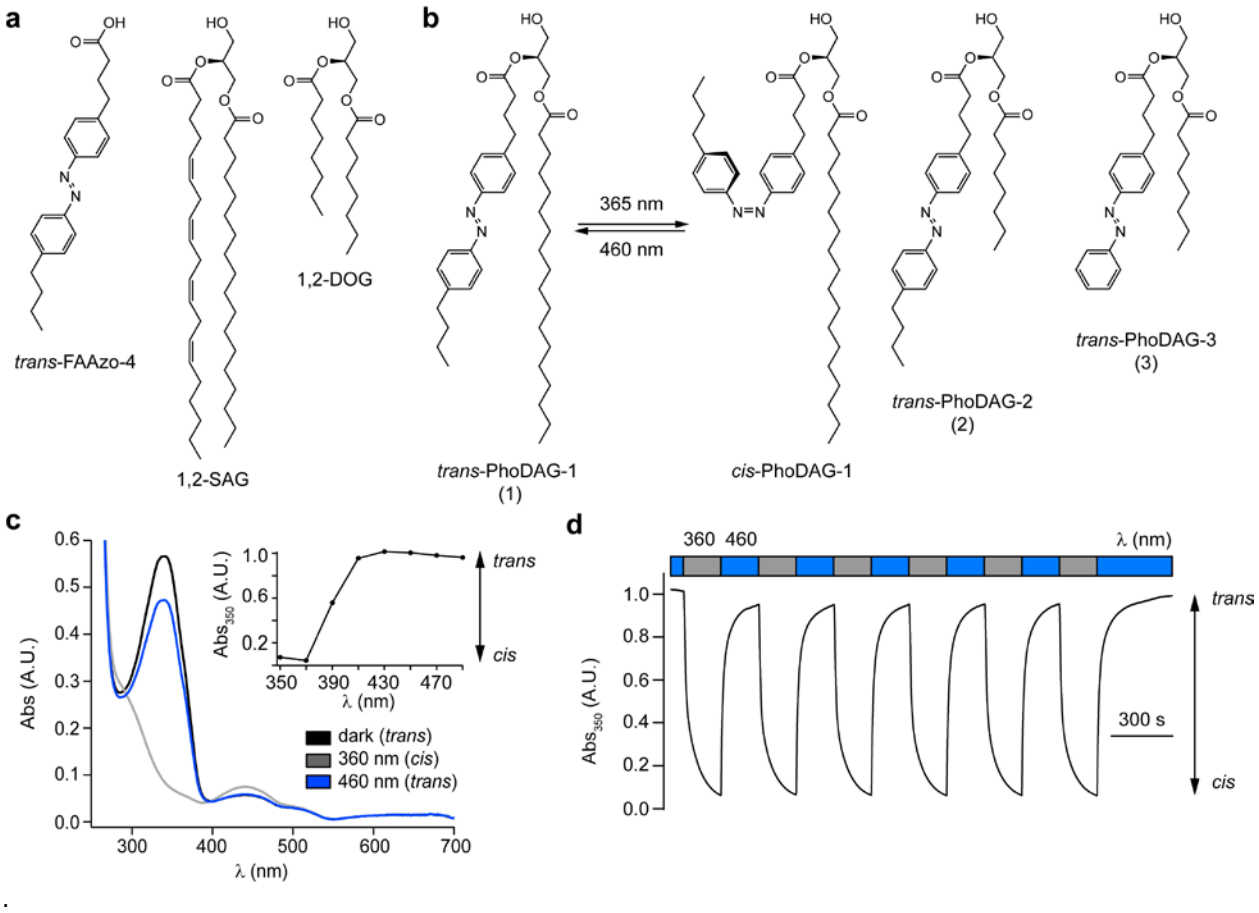

.

Figure 1 | Design and synthesis of photoswitchable diacylglycerols. (**a**) The chemical structures of the photoswitchable fatty acid **FAAzo-4**, 2-*O*-arachidonyl-1-*O*-stearoyl-*sn*-glycerol (1,2-SAG) and 1,2-*O*-dioctanoyl-*sn*-glycerol (1,2-DOG). (**b**) The chemical structures of photoswitchable diacylglycerols **PhoDAG-1** (**1**), **PhoDAG-2** (**2**) and **PhoDAG-3** (**3**). (**c**) The UV-Vis spectra of **PhoDAG-1** (25 μM in DMSO) in its *dark*-adapted (black), *UV*-adapted (gray) and *blue*-adapted (blue) photostationary states. The absorbance at λ = 350 nm was plotted as a function of the irradiation wavelength, demonstrating that **PhoDAG-1** existed primarily in its *trans*- and *cis*-configurations under blue and UV-A irradiation, respectively. (**d**) **PhoDAG-1** was cycled between the two states over many cycles without fatigue. The absorbance at λ = 350 nm was plotted over multiple cycles of alternating UV-A and blue irradiation.

Optical control of C1 domain translocation

We evaluated the effects of the PhoDAGs in HeLa cells transiently expressing a fluorescent C1 domain translocation reporter (C1-GFP)[17,18] (**Supplementary Table 1**). Before the addition of any compound, C1-GFP was evenly distributed within the cytoplasm, and the application of *trans*-**PhoDAG-1** did not affect its localization (**Fig. 2a**). Illumination with UV-A light (λ = 375 nm) and isomerization to *cis*-**PhoDAG-1** rapidly induced the translocation of C1-GFP towards the plasma membrane (**Fig. 2b**, **Supplementary Fig. 1**,**2**). After termination of the irradiation, C1-GFP diffused back into the cytoplasm, and translocation was again triggered on repeated stimulation (**Fig. 2c**). C1-GFP localization could be controlled with a high degree of spatial precision, as only cells that were directly irradiated were affected (**Supplementary Fig. 3**). Shorter UV-A pulses triggered a small and transient translocation, while longer periods of irradiation caused a larger and more sustained response (**Fig. 2d**), permitting the generation of oscillation patterns. After incubation with **PhoDAG-1** followed by washing and removal of extracellular compound, translocation of C1-GFP was still observed on photoactivation (**Supplementary Fig. 4a**). The magnitude of the translocation induced by *cis*-**PhoDAG-1** was comparable to that triggered by the uncaging of 1,2-DOG from its coumarin-caged form, *cg*-1,2-DOG (**Supplementary Fig. 4b-d**).

Interestingly, **PhoDAG-2** and **PhoDAG-3** did not induce pronounced translocation of C1-GFP towards the plasma membrane. Instead, C1-GFP mostly accumulated on the inner membranes on PhoDAG application (**Supplementary Fig. 5a**). We monitored the localization and uptake of the PhoDAGs by exploiting the quenching of coumarin fluorescence by the azobenzene. We loaded HeLa cells with coumarin-labelled arachidonic acid (*cg*-AA) (**Supplementary Fig. 5b**), which localizes predominantly at the inner cellular membranes[19]. Application of **PhoDAG-1** caused a slow but small decrease in the observed coumarin fluorescence (<20% of total, τ = 295 s) (**Fig. 2e** black, **Supplementary Fig. 5c**). In comparison, **PhoDAG-3** caused a more rapid and significant decrease in coumarin fluorescence (>70% in total, τ = 85 s) (**Fig. 2e** gray, **Supplementary Fig. 5d**). These results suggest that **PhoDAG-1** internalizes more slowly and remains trapped on the plasma membrane, while **PhoDAG-3** quickly diffuses and accumulates at inner membranes. UV-A irradiation alone did not trigger the translocation of C1-GFP to the plasma membrane (**Supplementary Fig. 6a**).

PhoDAGs modulate intracellular Ca^{2+} levels in HeLa cells

1,2-SAG was previously reported to increase intracellular Ca^{2+} ($[Ca^{2+}]_i$) levels in HeLa cells via activation of TRPC channels[11]. Using the genetically encoded Ca^{2+} sensor, R-GECO[20], we observed that application of *trans*-**PhoDAG-1** stimulated a small rise in $[Ca^{2+}]_i$ (**Fig. 2f**). Upon isomerization to *cis*-**PhoDAG-1**, a much larger $[Ca^{2+}]_i$ increase was observed. The TRPC channel blocker SKF-96365 suppressed the rise in $[Ca^{2+}]_i$ (**Fig. 2f**). After incubation with **PhoDAG-1** followed by washing and removal of extracellular compound, an increase in $[Ca^{2+}]_i$ was still observed on photoactivation (**Fig. 2g**, **Supplementary Fig. 4a**,**6b**). Incubation with cyclopiazonic acid, which depletes endoplasmic reticulum (ER) Ca^{2+} stores[21], diminished the Ca^{2+} response (**Fig. 2g**, orange). $NiCl_2$ in combination with a Ca^{2+}-free extracellular buffer[11] abolished the Ca^{2+} signal by preventing the entry of extracellular Ca^{2+} (**Fig. 2g**, gray). Together, these results suggest that *cis*-**PhoDAG-1** promotes Ca^{2+} influx by activation of TRPC3 and/or TRPC6 channels, which in turn triggers Ca^{2+}-induced Ca^{2+} release from intracellular stores. Interestingly, application and photoactivation of **PhoDAG-3** only caused a small increase in $[Ca^{2+}]_i$, which was not affected by SKF-96365 (**Supplementary Fig. 6c**).

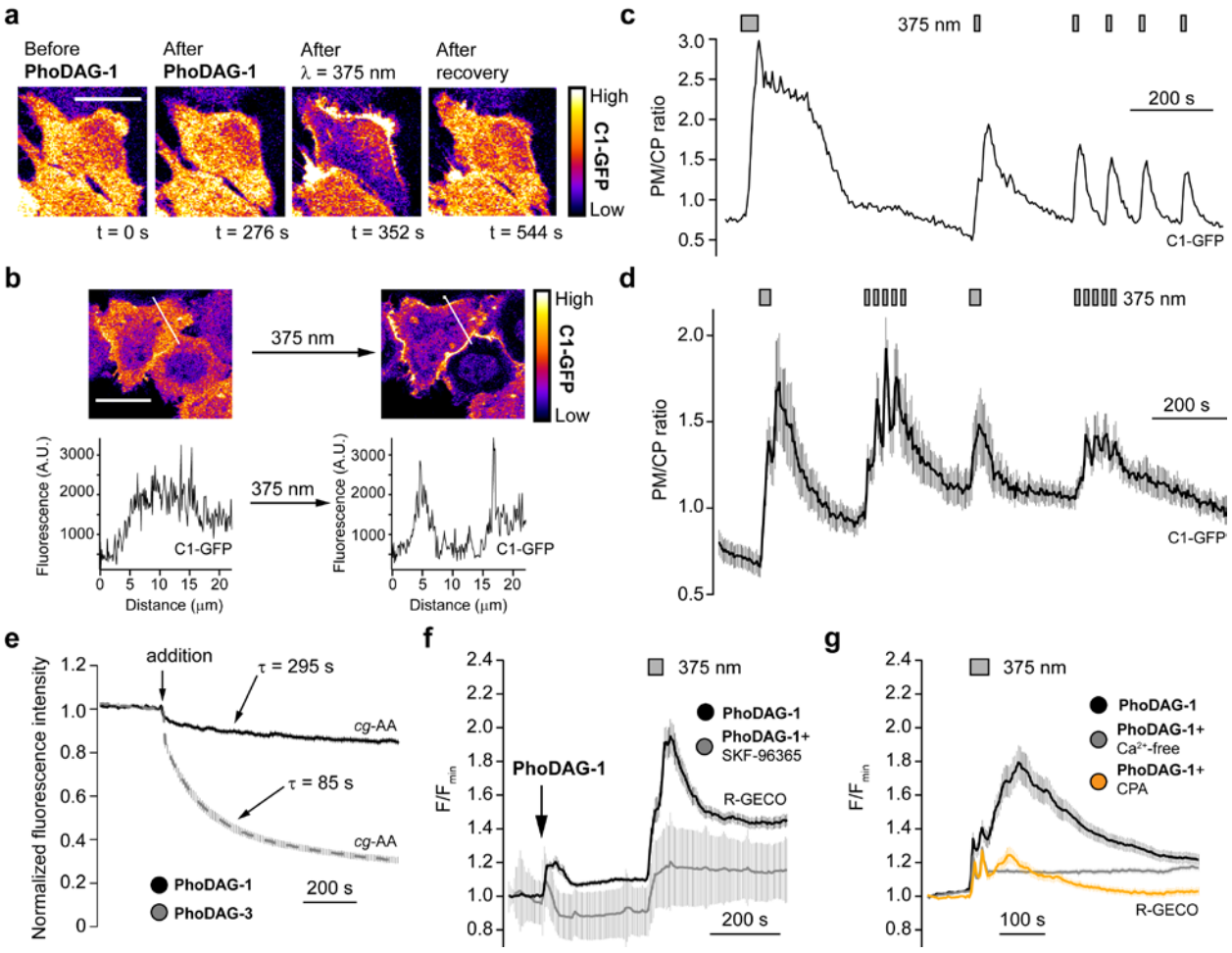
a
Before PhoDAG-1
After PhoDAG-1
After λ = 375 nm
After recovery
High
C1-GFP
Low
t = 0 s
t = 276 s
t = 352 s
t = 544 s
b
375 nm
High
C1-GFP
Low
Fluorescence (A.U.)
C1-GFP
Distance (μm)
375 nm
c
375 nm
200 s
PM/CP ratio
C1-GFP
d
375 nm
200 s
PM/CP ratio
C1-GFP
e
addition
τ = 295 s
cg-AA
τ = 85 s
cg-AA
Normalized fluorescence intensity
PhoDAG-1
PhoDAG-3
200 s
f
375 nm
PhoDAG-1
PhoDAG-1+ SKF-96365
PhoDAG-1
R-GECO
200 s
g
375 nm
PhoDAG-1
PhoDAG-1+ Ca2+-free
PhoDAG-1+ CPA
R-GECO
100 s

Figure 2 | PhoDAG-1 enables optical control of C1-GFP translocation and intracellular Ca^{2+} concentration in HeLa cells. (**a**) Fluorescence images showed that **PhoDAG-1** (150 μM) promotes reversible translocation of C1-GFP in HeLa cells towards the plasma membrane only after irradiation with λ = 375 nm light. (**b**) C1-GFP fluorescence intensity was measured across a representative cell (white line) loaded with **PhoDAG-1** before (left image) and after (right image) illumination with λ = 375 nm light. All scale bars = 20 μM. (**c**) Translocation could be triggered over multiple cycles in the presence of **PhoDAG-1**, and was quantified by plotting the plasma membrane to cytoplasm (PM/CP) fluorescence intensity ratio of a representative cell. (**d**) Patterns of C1-GFP translocation were generated by irradiation at λ = 375 nm in the presence of **PhoDAG-1** (n = 16, 2 experiments). (**e**) Fluorescence quenching dynamics of coumarin-labelled arachidonic acid (*cg*-AA, 100 μM) localized at the internal cell membranes after application of **PhoDAG-1** (150 μM, n = 18, 2 experiments, black) or **PhoDAG-3** (150 μM, n = 19, 2 experiments, gray). (**f**) The TRPC channel blocker SKF-96365 (50 μM) decreased the Ca^{2+} influx on application and photoactivation of **PhoDAG-1** (n = 54, 2 experiments, gray) when compared to **PhoDAG-1** alone (n = 16, 2 experiments, black). $[Ca^{2+}]_i$ levels were monitored with the R-GECO Ca^{2+} sensor. (**g**) After incubation with **PhoDAG-1** followed by the removal of extracellular compound, both cyclopiazonic acid (CPA, 50 μM, n = 64, 4 experiments, orange) and $NiCl_2$ (5 mM) combined with a Ca^{2+}-free extracellular buffer (0.1 mM EGTA, n = 73, 4 experiments, gray) reduced the Ca^{2+} response. Error bars were calculated as s.e.m.

Optical control of protein kinase C

PKCs are a group of serine/threonine kinases that are involved in cell cycle regulation, proliferation, apoptosis and migration[3]. The PKC family is grouped into three different subtypes; conventional, novel and atypical, according to their cofactor requirements as determined by the regulatory elements linked to the kinase domain[22]. These regulatory domains allow different PKC isoforms to decode different signals at the plasma membrane, such as the generation of DAG.

Novel PKCs, such as PKCδ, contain two C1 domains that orchestrate their activation alongside translocation toward the plasma membrane in a Ca^{2+}-independent fashion[23]. In HeLa cells, **PhoDAG-1** triggered translocation of fluorescently labeled PKCδ (PKCδ-RFP) towards the plasma membrane following a UV-A flash (**Fig. 3a, Supplementary Movie 1**). After termination of the irradiation, PKCδ-RFP translocated back to the cytosol with a τ-value of ~102 s (**Fig. 3b**). Translocation could be repeated over several cycles, however the magnitude of translocation often diminished with repeated UV-A flashes of the same duration (**Supplementary Fig. 7a**). To overcome this limitation, we developed a protocol that allowed us to perform many translocation cycles without a decrease in efficiency by increasing the irradiation time on each sequential photostimulation (**Fig. 3c**). Increasing the interval time between the UV-A pulses did not affect the translocation magnitude, suggesting that *trans*-**PhoDAG-1** metabolism was not a significant factor (**Supplementary Fig. 7b**).

Conventional PKCs, such as PKCα, were also placed under optical control. **PhoDAG-1** triggered the translocation of PKCα-GFP[24] towards the plasma membrane on photoactivation (**Supplementary Fig. 7c**). In contrast to C1-GFP and PKCδ-RFP, PKCα-GFP translocation efficiency decreased quickly alongside Ca^{2+}-influx on sequential photostimulations, reflecting its known Ca^{2+}-sensitivity[22].

Although PKC translocation to the plasma membrane is normally associated with its activation[25], translocation alone is not sufficient to conclude whether **PhoDAG-1** can trigger PKC phosphorylation. To this end, we utilized the C kinase activity reporter (CKAR)[26], which displays a decrease in FRET efficiency on phosphorylation (**Fig. 3d,e**). In line with previous reports[26], the addition of 1,2-DOG (**Supplementary Fig. 7d**) to HeLa cells expressing CKAR caused a 5.5% increase in the CFP/YFP

fluorescence ratio, while the application of phorbol 12-myristate 13-acetate (PMA) (**Supplementary Fig. 7e**) caused a 4.8% increase. The application of *trans*-**PhoDAG-1** did not cause a significant CKAR FRET change. However, a 4.4% increase in the CFP/YFP fluorescence ratio was observed on isomerization to *cis*, corresponding to 80% of the response evoked by 1,2-DOG (**Fig. 3e**). The application of *trans*-**PhoDAG-3** also caused a small increase (2.2%) in the CFP/YFP ratio on application, and a further 2.0% increase was induced by photoactivation (**Supplementary Fig. 7f,g**). The overall response after the application and photoactivation of **PhoDAG-3** was similar to that which was evoked by **PhoDAG-1** (95%) or 1,2-DOG (76%). Interestingly, this effect was observed even in the absence of a clear translocation to the outer plasma membrane, suggesting that PKCδ-RFP could be activated on internal membranes as well. In all cases, the effect was reversed by the application of the broad-spectrum PKC inhibitors Gö-6983 or chelerythrine chloride (**Fig. 3d,e**, **Supplementary Fig. 7d**–**h**)[27,28].

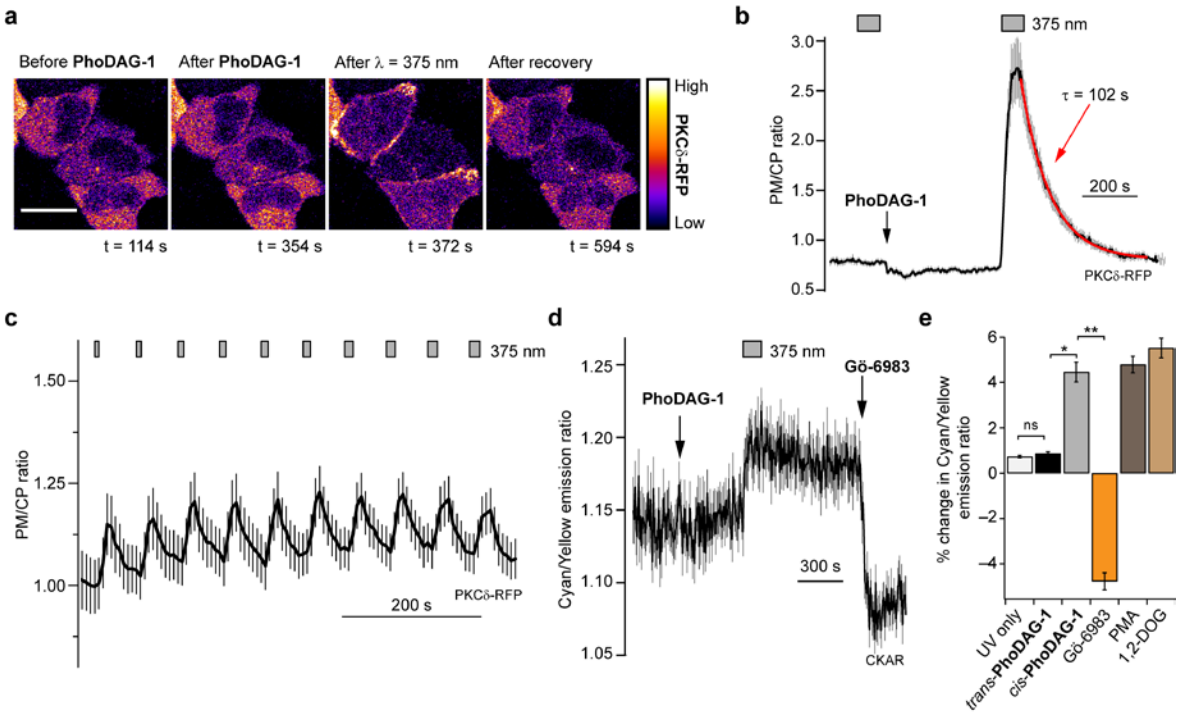

Figure 3 | **PhoDAG-1 enables optical control of PKC.** (**a**) Fluorescence images of HeLa cells expressing PKCδ-RFP showed that **PhoDAG-1** (100 μM) triggered reversible translocation of PKCδ-RFP towards the plasma membrane on λ = 375 nm irradiation. Scale bar = 20 μM. (**b**) After photoactivation, PKCδ-RFP redistributed back to the cytoplasm (n = 19, 2 experiments). Translocation was quantified as the plasma membrane to cytoplasm (PM/CP) fluorescence intensity ratio. (**c**) Oscillations of PKCδ-RFP translocation were generated by sequential pulses of UV-A irradiation with increasing length (n = 11 cells, 1 representative experiment). (**d,e**) PKC activation was evaluated in HeLa cells expressing PKCδ-RFP and the cytosolic C kinase activation reporter, CKAR[26]. (**d**) **PhoDAG-1** (300 μM) triggered an increase in the cyan/yellow fluorescence emission ratio on isomerization to *cis* (n = 49, 3 experiments). (**e**) Photoactivation of **PhoDAG-1** (n = 49, 3 experiments) produced a similar FRET change when compared to 1,2-DOG (300 μM, n = 32, 1 experiment) and PMA (5 μM, n = 31, 2 experiments). Application of Gö-6983 (10 μM, n = 49, 3 experiments) reversed this effect. The Mann-Whitney test was used to determine statistical significance. ns = not significant $P>0.05$, *$P<0.005$, ** $P<0.001$. Error bars were calculated as s.e.m.

Optical control of Ca^{2+} oscillations in β-cells

In pancreatic β-cells, glucose induces oscillations in $[Ca^{2+}]_i$ levels, the frequency of which strongly correlate with insulin secretion[29]. Similarly, DAG levels are known to oscillate in β-cells[18], implicating a connection between glucose and lipid metabolism. The exact mechanism by which DAGs regulate insulin secretion remains elusive, however increased DAG levels were reported to terminate Ca^{2+} oscillations in the mouse insulinoma-derived β-cell line, MIN6[30,31]. The addition of *trans*-**PhoDAG-1** did not affect Ca^{2+} oscillations in MIN6 cells stimulated by a high glucose concentration (20 mM). Photoactivation with λ = 375 nm for 3 min caused a rapid decline in both the intensity and frequency of the Ca^{2+} oscillations (**Fig. 4a**,**b**), as well as the overall $[Ca^{2+}]_i$ level (**Supplementary Fig. 8a**). In the majority of cells examined, this termination was transient and lasted on average 5 min. **PhoDAG-3** behaved in a similar manner, but was active at a much lower concentration (**Fig. 4c**).

Ca^{2+} oscillations in β-cells are driven by a dynamic interplay between voltage-gated ion channels. DAGs modulate the conductance of L-type voltage-activated Ca^{2+} channels (Ca_v) in mouse β-cells, and 1,2-DOG is known to inhibit the whole-cell Ca_v current[32]. Using whole-cell patch clamp electrophysiology in MIN6 cells, we evaluated the effects of PhoDAGs on Ca_v conductance. Photoactivation of **PhoDAG-3** with UV-A light triggered a decrease in the Ca_v current (**Fig. 4d**, **Supplementary Fig. 8b**). This effect could be reversed by irradiation with blue light, and could be repeated over several cycles (**Fig. 4e**). Application of diltiazem, which blocks L-type Ca^{2+} channels, diminished the Ca_v current in a similar fashion (**Supplementary Fig. 8c**). UV-A irradiation alone did not affect the oscillatory behavior (**Supplementary Fig. 9**) or the Ca_v current (**Supplementary Fig. 8c**).

To compare the responses observed in MIN6 to those of primary β-cells, we cultured β-cells from dissociated mouse pancreatic islets. As in MIN6 cells, **PhoDAG-3** triggered a light-dependent decrease in Ca^{2+} oscillation frequency (**Fig. 4f**) and the whole-cell Ca_v conductance (**Fig. 4g**). Surprisingly, in these cells *cis*-**PhoDAG-1** caused an increase in the oscillation frequency and $[Ca^{2+}]_i$ level (**Fig. 4h**). Patch clamp experiments revealed that, whereas photoactivation of **PhoDAG-1** had little effect on Ca_v

conductance (**Supplementary Fig. 10a**), it caused a reduction in the conductance of delayed rectifier voltage-gated K^+ channels (K_v) (**Fig. 4i**). Ablation of K_v has been shown to increase Ca^{2+} fluxes in β-cells by extending the action potential duration[33]. Similar effects can be also induced by arachidonic acid, which is known to block $K_v2.1$ channels[34]. In control experiments, the application of 1,2-DOG indeed decreased the magnitude of β-cell Ca_v conductance (**Supplementary Fig. 10b**), while the addition of arachidonic acid reduced the K_v current (**Supplementary Fig. 10c**). Neither UV-A nor blue-irradiation alone affected the Ca_v or K_v currents (**Supplementary Fig. 10b,c**).

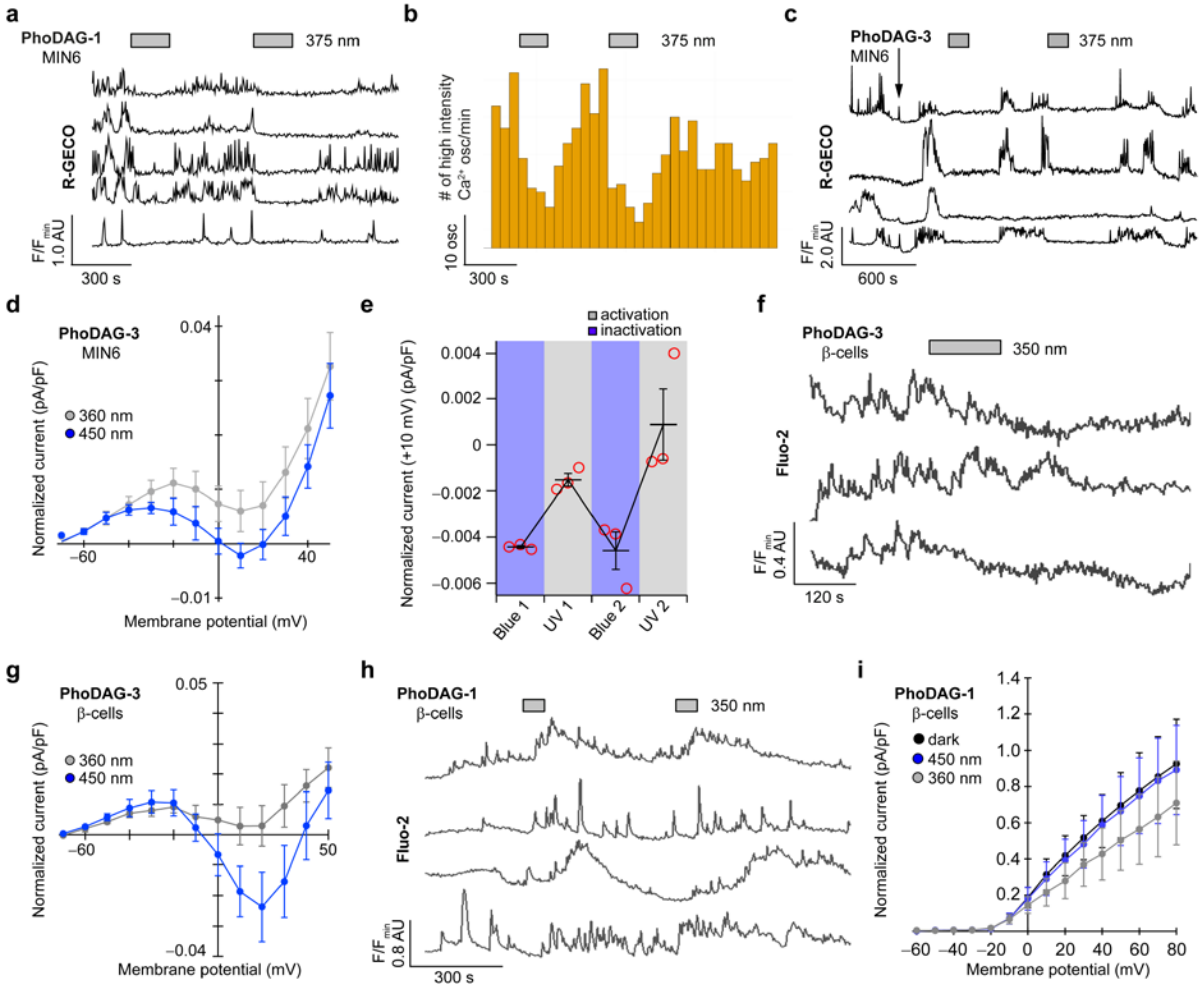
a
PhoDAG-1
MIN6
375 nm
R-GECO
F/F min
1.0 AU
300 s
b
375 nm
# of high intensity Ca2+ osc/min
10 osc
300 s
c
PhoDAG-3
MIN6
375 nm
R-GECO
F/F min
2.0 AU
600 s
d
PhoDAG-3
MIN6
360 nm
450 nm
Normalized current (pA/pF)
0.04
−0.01
−60
40
Membrane potential (mV)
e
activation
inactivation
Normalized current (+10 mV) (pA/pF)
0.004
0.002
0
−0.002
−0.004
−0.006
Blue 1
UV 1
Blue 2
UV 2
f
PhoDAG-3
β-cells
350 nm
Fluo-2
F/F min
0.4 AU
120 s
g
PhoDAG-3
β-cells
360 nm
450 nm
Normalized current (pA/pF)
0.05
−0.04
−60
50
Membrane potential (mV)
h
PhoDAG-1
β-cells
350 nm
Fluo-2
F/F min
0.8 AU
300 s
i
PhoDAG-1
β-cells
dark
450 nm
360 nm
Normalized current (pA/pF)
1.4
1.2
1.0
0.8
0.6
0.4
0.2
−60 −40 −20 0 20 40 60 80
Membrane potential (mV)

Figure 4 | **Optical control of Ca^{2+} oscillations in MIN6 and dissociated primary mouse β-cells.** (**a-c**) Ca^{2+} oscillations in glucose-stimulated (20 mM) MIN6 cells were monitored using R-GECO. **PhoDAG-1** (300 μM) decreased $[Ca^{2+}]_i$ levels on photoactivation with λ = 375 nm light, displayed as (**a**) individual $[Ca^{2+}]_i$ traces from four representative cells, and (**b**) a statistical analysis of the oscillation frequency (n = 38, 3 experiments). Bar graphs represent the number of high intensity Ca^{2+} oscillations (>50% of highest transient in each trace) detected within every 60 s interval. (**c**) **PhoDAG-3** (35 μM) also triggered a decrease in glucose-stimulated (20 mM) Ca^{2+} oscillations on photoactivation. (**d**) Isomerization to *cis*-**PhoDAG-3** (35 μM, n = 6) induced a decrease in whole-cell voltage-gated Ca^{2+} channel (Ca_v) current. (**e**) This effect was reversed by blue light and could be repeated over several cycles (n = 3). (**f-i**) In dissociated mouse β-cells: (**f**) *cis*-**PhoDAG-3** (10 μM) caused a decrease in glucose-stimulated (11 mM) Ca^{2+} oscillations, corresponding to (**g**) a reduction in the Ca_v current (15 μM, n = 3). (**h**) In contrast, *cis*-**PhoDAG-1** (200 μM) led to an increase in the Ca^{2+} oscillation frequency. (**i**) A reduction in the delayed rectifier voltage-activated K^+ channel (K_v) current was observed on isomerization to *cis*-**PhoDAG-1** (n = 3). Error bars were calculated as s.e.m.

Optical control of insulin secretion in pancreatic islets

Islets of Langerhans are endocrine micro-organs comprised of hundreds of β-cells together with α-, δ- and pancreatic polypeptide cells[35]. We therefore examined whether responses in intact islets were similar to MIN6 and dissociated β-cells. In contrast to the effects observed in dissociated cells, intact mouse pancreatic islets pre-treated with either **PhoDAG-1** (**Fig. 5a,b**) or **PhoDAG-3** (**Supplementary Fig. 11a,b**) responded to illumination with a marked and reproducible increase in the glucose-stimulated (11 mM) Ca^{2+} oscillation frequency. These results could be mimicked by the application of 1,2-DOG (**Fig. 5c**). Strikingly, islets treated with **PhoDAG-1** were rendered light-responsive, displaying almost a 3-fold increase in insulin secretion (at 16.7 mM glucose) following photoactivation (**Fig. 5d**). UV-A irradiation alone did not significantly affect Ca^{2+} oscillation frequency or the amount of insulin secreted (**Supplementary Fig. 11c,d**). These results suggest that photoactivation of the PhoDAGs in intact pancreatic islets increases the Ca^{2+} oscillation frequency, and consequently elevates insulin secretion.

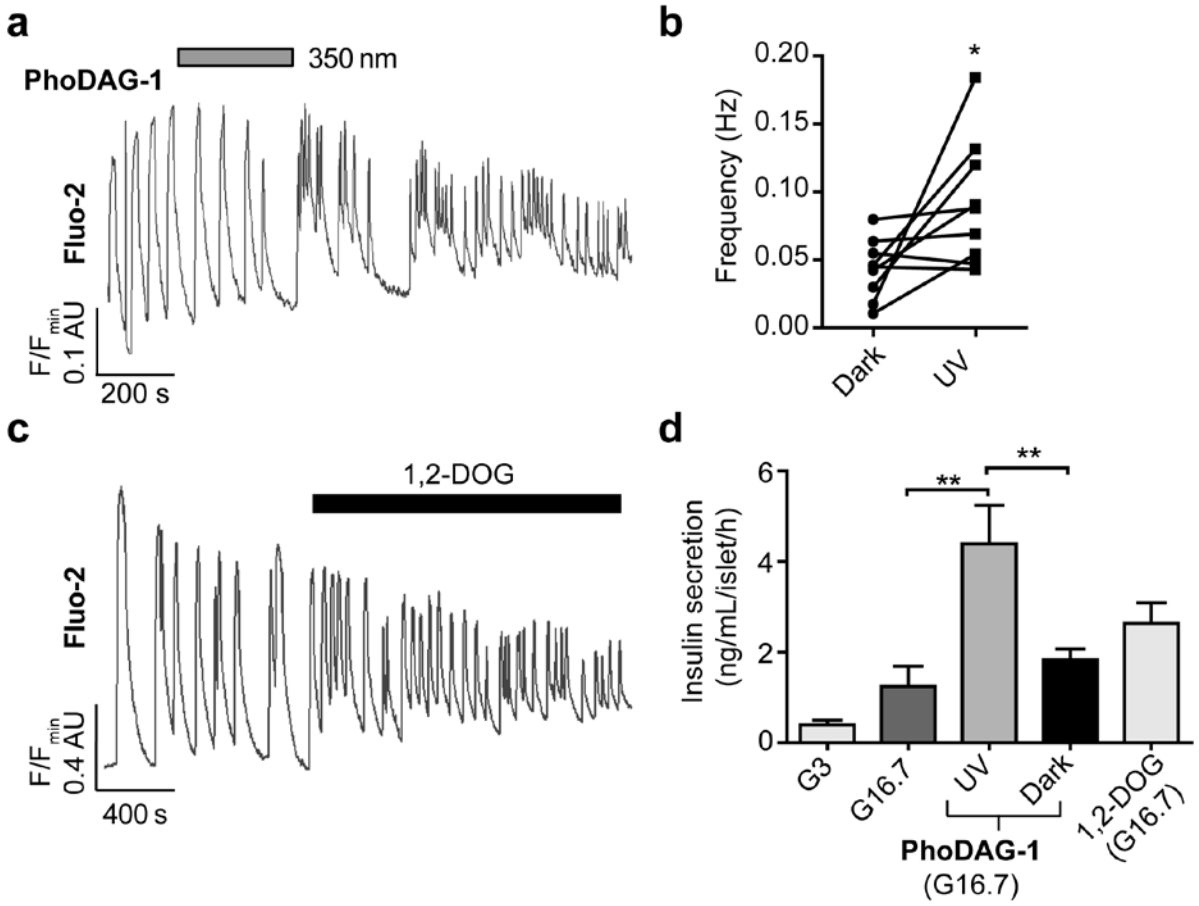

Figure 5 | **Optical control of insulin secretion in intact mouse pancreatic islets.** Glucose-stimulated (11 mM) Ca^{2+} oscillations in whole mouse pancreatic islets were monitored using Fluo-2. (**a,b**) Photoactivation of **PhoDAG-1** (200 μM) triggered an increase in the oscillation frequency, displayed as (**a**) a representative trace from a single islet and (**b**) the average oscillation frequencies for several islets before and after λ = 350 nm irradiation (n = 9 recordings from 4 animals). (**c**) The application of 1,2-DOG (100 μM) led to an increase in the oscillation frequency (n = 8 recordings from 4 animals). (**d**) As determined by a homogeneous time-resolved fluorescence (HTRF) assay, *cis*-**PhoDAG-1** (200 μM) at 16.7 mM glucose led to a 3-fold increase in insulin secretion when compared to either *trans*-**PhoDAG-1** or glucose-stimulated conditions (16.7 mM) alone. Similar effects were observed with 1,2-DOG (100 μM) (n = 3 assays from 6 animals). G3 = 3 mM glucose, G16.7 = 16.7 mM glucose. The Mann-Whitney test was used to determine statistical significance. ns = not significant, *P<0.05, **P<0.01. Error bars were calculated as s.e.m.

Optical control of synaptic transmission

DAG is known as a regulator of neuronal activity[9,36]. Multiple downstream effectors of DAG signaling have been described[37], including the PKC-dependent phosphorylation of Munc18 and the direct binding of DAG to Munc13 proteins, and have been linked to an increase in synaptic transmission[38,39]. Munc13s function as essential priming factors for synaptic vesicles, preparing them for fusion with the plasma membrane at the active zone, thereby facilitating the release of neurotransmitters into the synaptic cleft[40–42]. We found that **PhoDAG-1** could indeed trigger the translocation of the fluorescent translocation reporter Munc13-1-GFP towards the plasma membrane on photoactivation in HeLa cells over multiple cycles (**Fig. 6a**). The DAG-insensitive Munc13-1^{H567K}-GFP mutant reporter[40] did not respond to **PhoDAG-1** (**Supplementary Fig. 12**).

We then examined the effects of all three PhoDAGs in primary cultures of mouse autaptic hippocampal neurons. In this case, **PhoDAG-2** produced the most dramatic and reproducible effect on synaptic transmission. Synaptic transmission was measured by recording evoked excitatory postsynaptic currents (EPSCs) that were elicited by depolarization-induced action potentials. The initial EPSC amplitude was not affected by the presence of *trans*-**PhoDAG-2** when compared to control neurons (**Fig. 6b**). However, on activation with λ = 365 nm light (30 s), we observed a prominent increase in the EPSC amplitude (**Fig. 6c,d**). This activation was sustained until inactivation with λ = 425 nm light (20 s), which triggered a rapid and significant decrease of the EPSC amplitude. This effect was absent in control neurons and could be repeated over multiple cycles with little to no decay in efficacy. The first activation of **PhoDAG-2** led to a 1.19±0.07-fold increase of the EPSC amplitude, and was similar in the following two rounds of activation (1.19±0.1 fold and 1.18±0.07 fold) (**Fig. 6e**). Similarly, the first inactivation led to a 0.80±0.03 fold decrease in the EPSC amplitude, and was similar in the two following cycles (0.77±0.03 and 0.76±0.03 fold respectively). We did not observe any change in the series resistance of the patch pipette during activation or inactivation of **PhoDAG-2**, which could have generated artifacts mimicking changes in the EPSC size (**Supplementary Fig. 13**). Similarly, **PhoDAG-2** affected the frequency of spontaneous miniature postsynaptic currents (sEPSCs), pointing to an acute effect on the presynaptic release machinery (**Fig. 6f**). An increase in the sEPSC frequency was observed during periods of

activation, by 1.68±0.3, 1.55±0.4 and 1.62±0.2 fold over three rounds. Inactivation led to a decrease in the sEPSC frequency, by 0.65±0.1, 0.82±0.14, and 0.63±0.06 fold over three inactivation cycles, respectively. **PhoDAG-3** produced similar results (**Supplementary Fig. 14**), however the variability of the response of the neurons to photoactivation was larger, and some neurons did not respond consistently during all rounds of activation/inactivation. **PhoDAG-1** did not yield a consistent effect on synaptic transmission, likely due to its limited solubility at these high concentrations during incubation.

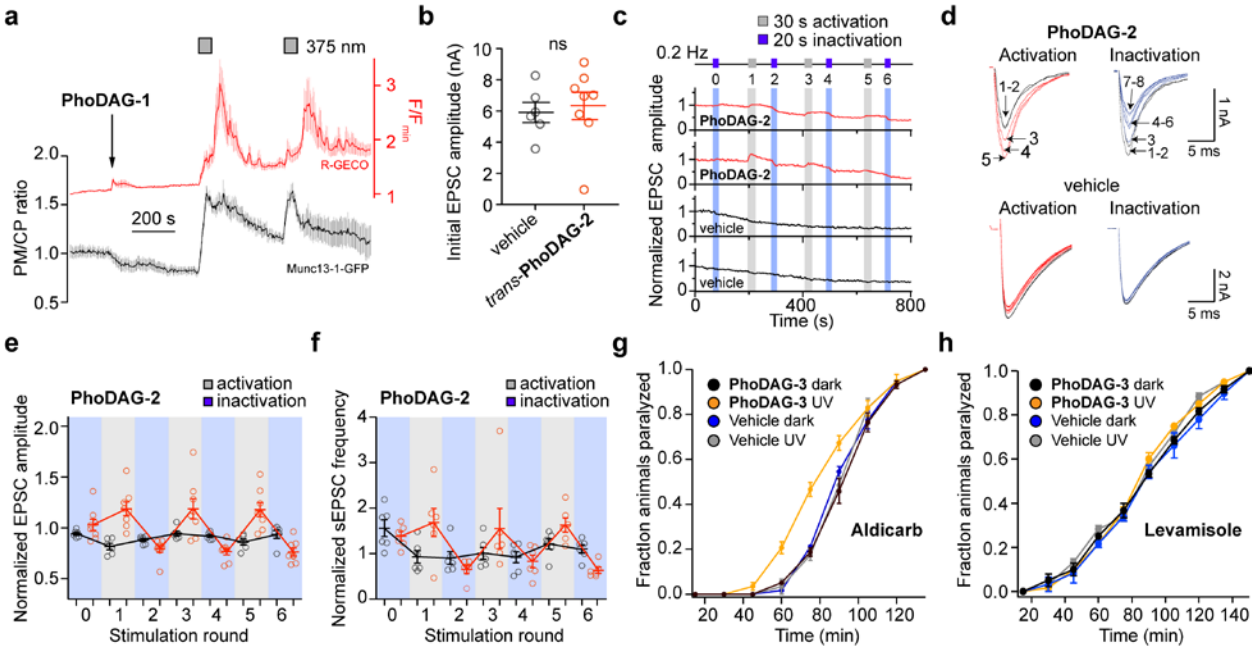
a
375 nm
PhoDAG-1
R-GECO
200 s
Munc13-1-GFP
PM/CP ratio
F/F min
b
ns
Initial EPSC amplitude (nA)
vehicle
trans-PhoDAG-2
c
30 s activation
20 s inactivation
0.2 Hz
PhoDAG-2
vehicle
Normalized EPSC amplitude
Time (s)
d
PhoDAG-2
Activation
Inactivation
vehicle
1 nA
2 nA
5 ms
e
PhoDAG-2
activation
inactivation
Normalized EPSC amplitude
Stimulation round
f
PhoDAG-2
activation
inactivation
Normalized sEPSC frequency
Stimulation round
g
PhoDAG-3 dark
PhoDAG-3 UV
Vehicle dark
Vehicle UV
Fraction animals paralyzed
Aldicarb
Time (min)
h
PhoDAG-3 dark
PhoDAG-3 UV
Vehicle dark
Vehicle UV
Fraction animals paralyzed
Levamisole
Time (min)

Figure 6 | PhoDAGs enable optical control of Munc13 and synaptic transmission. (**a**) In HeLa cells, **PhoDAG-1** (150 μM) triggered reversible translocation of Munc13-1-GFP on photoactivation (n = 14, 3 experiments). (**b**-**f**) Mouse hippocampal neurons were pre-incubated with **PhoDAG-2** (500 μM, 20–25 min, 37 ˚C) and excitatory post synaptic currents (EPSCs) were monitored by whole-cell voltage clamp electrophysiology. (**b**) *trans*-**PhoDAG-2** (red, n = 8) did not affect the EPSC amplitude when compared to control neurons (black, n = 6). (**c**) Photoactivation of **PhoDAG-2**-treated neurons with λ = 365 nm light caused an increase in the EPSC amplitude, while deactivation with λ = 425 nm light reversed the effect. Shown are two neurons pre-incubated with **PhoDAG-2** (red) and two control neurons (black). (**d**) Representative EPSC traces during activation and inactivation. Numbers indicate the EPSC number. Black traces are the EPSC before irradiation. (**e,f**) The normalized change in (**e**) the EPSC amplitude (red = **PhoDAG-2**, n = 8; black = vehicle, n = 6) and (**f**) sEPSC frequency (red = **PhoDAG-2**, n = 6; black = vehicle, n = 6) over six rounds of alternating activation and inactivation. Values for individual neurons are presented as open circles. (**g**) *cis*-**PhoDAG-3** (1 mM) increased the rate of aldicarb-induced (1 mM) paralysis in *Caenorhabditis elegans* (n = 3 experiments, 20 animals each) when compared to animals exposed to *trans*-**PhoDAG-3** (black). The paralysis rate was not affected by UV-A irradiation alone (blue, gray). (**h**) *cis*-**PhoDAG-3** (1 mM) did not affect the rate of levamisole-induced (0.1 mM) paralysis in *C. elegans* (n = 3 experiments, 20 animals each) when compared to animals exposed to *trans*-**PhoDAG-3** (black). The paralysis rate was not affected by UV-A irradiation alone (blue, gray). A Mann-Whitney test was used to determine statistical significance. Error bars were calculated as s.e.m.

Control of *Caenorhabditis elegans* synaptic transmission

Caenorhabditis elegans has been used extensively to study synaptic transmission[43]. At the neuromuscular junction, acetylcholine is released from cholinergic motor neurons and activates post-synaptic cholinergic receptors of the body-wall muscles, inducing muscle contraction[44]. This process is terminated by the action of acetylcholinesterase. Sensitivity to aldicarb, an acetylcholinesterase inhibitor, is therefore commonly used to study synaptic transmission at the neuromuscular junction[45]. *C. elegans* become hypersensitive to aldicarb under conditions of excess acetylcholine release and display a faster onset of paralysis on exposure to the drug. Animals cultivated in the presence of *cis*-**PhoDAG-3** (1 mM) showed a faster onset of paralysis induced by aldicarb (1 mM) as compared to animals cultivated only with ethanol (vehicle), with or without UV-A irradiation. Animals that were exposed to *trans*-**PhoDAG-3** showed no aldicarb hypersensitivity (**Fig. 6g**). To exclude post-synaptic effects (e.g. a possible **PhoDAG-3**-induced increase in the sensitivity of nicotinic acetylcholine receptors (nAChRs)), we used levamisole, which paralyzes animals due to hyperstimulation of muscle-specific nAChRs[46,47]. Animals grown in the presence of *trans*- or *cis*-**PhoDAG-3** showed similar rates of levamisole-induced paralysis when compared to the vehicle controls (**Fig. 6h**). These results suggest that **PhoDAG-3** affects pre-synaptic transmission via modulating neurotransmitter release at the *C. elegans* neuromuscular junction.

DISCUSSION

Here, we have demonstrated that the three PhoDAGs are versatile tools for controlling DAG signaling in a variety of experimental settings, and can even be applied *in vivo*. In all cases, the PhoDAGs were more potent in their *cis*-configuration, which is characterized by an increased molecular dipole moment and a more bent orientation[48]. We hypothesize that these changes mimic the transition from a less bent (ex. saturated) fatty acid, to a highly bent acyl chain like arachidonic acid. Effectively, this action mimics an increase in DAG levels on the membrane, potentially by making the headgroup more accessible for C1 domain binding.

The length of each acyl chain is crucial, as hydrophobicity determines the localization and site of activity. We envision that **PhoDAG-1** could be used as a general tool, by virtue of C1-fusion, to translocate other effector proteins towards the plasma membrane in a reversible manner. This approach can be extended to other kinases, lipases, or glycosidases, and could be invaluable in understanding how plasma membrane localization affects these proteins. Although the shorter chain PhoDAGs triggered translocation towards intracellular membranes preferentially, we demonstrated that this does not limit their utility in other settings. As photochromic ligands, they are applied to cells extracellularly without the need for genetic manipulation. Although their activity cannot be genetically targeted to specific organelles, activation can still be induced with the spatial precision of light, enabling specific cells or organelles to be activated on command.

As with the metabolic generation of endogenous DAGs, the PhoDAGs stimulate a mosaic of effector proteins, similar to the downstream activation of the G_q-pathway. Although the small dynamic range of the CKAR sensor might limit our detection of PKC phosphorylation to quite low activation levels, our results in more complex systems suggest that the PhoDAGs indeed are capable of stimulating the cell in a physiologically relevant manner. In pancreatic β-cells, DAG signaling can be manipulated with a degree of precision and reproducibility currently unavailable to other chemical tools. These effects likely involve the activation of PKC alongside other partners including Munc13, affecting glucose-stimulated Ca^{2+} oscillations via effects on K_v/Ca_v channels, intracellular Ca^{2+} stores, the SNARE apparatus, granule

sensitivity and combinations thereof[49]. Similarly, our experiments in both hippocampal neurons and *C. elegans* suggest that the PhoDAGs increases neurotransmitter release by affecting the pre-synaptic release machinery. *cis*-PhoDAGs likely activate of Munc13 or cause the phosphorylation of Munc18[9,39], promoting vesicle release. Combined, these results demonstrate that the PhoDAGs are useful tools to study the effects of DAG on the exocytosis of both hormones and neurotransmitters.

Most notably, the PhoDAGs revealed the cell and tissue-context of DAG signaling in pancreatic β-cells. When PhoDAGs are activated on β-cell inner membranes, an overall decrease in the Ca^{2+} oscillation frequency is observed. Conversely, DAG-activation on the outer plasma membrane preferentially leads to an increase in oscillation speed. Similar effects were also observed for the uncaging of arachidonic acid on the inner vs outer membranes of MIN6 cells[19], which is not surprising given the metabolic connection between these two lipids. The divergent effects observed between MIN6 and dissociated β -cells highlight the importance of the acyl chain length for DAG activity. This may stem from subtle differences in ion channel expression, membrane composition, and endogenous DAG levels between immortalized and primary cells. In the case of intact islets, a greater amount of extracellular matrix likely increases the surface availability of both long- and short-chain PhoDAGs, resulting in a reduced effect on the Ca_v channels. This work highlights the limitations of model cell lines, and may explain some of the contrasting reports in the literature on the effects of DAG in pancreatic β-cells.

The PhoDAGs permit control over C1-containg proteins with unmatched spatiotemporal precision. They possess the main advantage of caged DAGs, as they can be applied to cells in the inactive *trans*-configuration where they can be switched ON in seconds with a light stimulus. Importantly, these small molecule tools stand alone in their ability to switch OFF. This characteristic will enable researchers to mimic the natural oscillations observed in both DAG levels and PKC activation, in a fully time-controlled fashion[26]. As the PhoDAGs require high energy UV-A irradiation to become activated, their use could be partially restricted to primary research applications due to the cytotoxicity associated with high intensity UV-A light. Future studies will be directed towards preparing “red-shifted” PhoDAGs[50], or those which can be activated by two-photon irradiation. This will permit the use of longer wavelength, and lower energy

irradiation for photoactivation. This deeper-penetrating light will increase the PhoDAGs applicability in more complex intact tissues, and as potential therapeutics.

As a lipid precursor, DAG is incorporated into a collection of more complicated glycerolipids that serve as structural components, protein anchors, and signaling molecules. We expect that novel photolipids built around the DAG scaffold will emerge as useful tools to control a variety of proteins, alongside the membranes with which they interact.

ACKNOWLEDGMENTS

DT and JAF gratefully acknowledge the Deutsche Forschungsgemeinschaft (SFB 1032 project B09, TRR 152) and the European Research Council (ERC Advanced Grant 268795 to DT) for financial support. CS is grateful for funding by the Deutsche Forschungsgemeinschaft (TRR 83). DAY acknowledges the EIPOD Programme at EMBL. DJH was supported by Diabetes UK R.D. Lawrence (12/0004431) and EFSD/Novo Nordisk Rising Star Fellowships, and an MRC Project Grant (MR/N00275X/1) with GAR. DJH and GAR were also supported by Imperial Confidence in Concept (ICiC) Grants. GAR was supported by Wellcome Trust Senior Investigator (WT098424AIA) and Royal Society Wolfson Research Merit Awards, by MRC Programme (MR/J0003042/1; MR/L020149/1; MR/L02036X/1), Biological and Biotechnology Research Council (BB/J015873/1) and Diabetes UK (11/0004210; 15/0005275) project grants. JN was supported by Deutsche Forschungsgemeinschaft (DFG) grants FOR1279 (GO1011/4-1 and 4-2) and Cluster of Excellence Frankfurt (EXC115) (to AG). We thank Dr. Martin Sumser, Dr. Johannes Broichhagen, and Dr. Timm Fehrentz for insightful discussions leading to the preparation of the manuscript; and Margherita Duca, Simone Wouters, Ryan Mitchell and Natalie Johnston for experimental assistance. We are grateful for the technical support of EMBL's Advanced Light Microscopy Facility.

AUTHOR CONTRIBUTIONS

DT and CS coordinated and supervised the study. JAF designed and synthesized the compounds. JAF, DAY, and DJH carried out imaging and secretion experiments. GAR provided reagents and assisted with data analysis. JAF and NL performed electrophysiological experiments. JN performed experiments in *C. elegans* under the supervision of AG. JSR and NB coordinated and supervised electrophysiological recordings. All authors contributed to writing the manuscript.

REFERENCES

1. Almena, M. & Mérida, I. Shaping up the membrane: diacylglycerol coordinates spatial orientation of signaling. *Trends Biochem. Sci.* **36,** 593–603 (2011).

2. Brose, N. & Rosenmund, C. Move over protein kinase C, you've got company: alternative cellular effectors of diacylglycerol and phorbol esters. *J. Cell Sci.* **115,** 4399–4411 (2002).

3. Newton, A. C. Protein Kinase C : Structure , Function , and Regulation. *J. Biol. Chem.* **270,** 28495–28498 (1995).

4. Pessin, M. S. & Raben, D. M. Molecular species analysis of 1,2-diglycerides stimulated by alpha-thrombin in cultured fibroblasts. *J. Biol. Chem.* **264,** 8729–8738 (1989).

5. Marignani, P. A., Epand, R. M. & Sebaldt, R. J. Acyl Chain Dependence of Diacylglycerol Activation of Protein Kinase C Activity in Vitro. *Biochem. Biophys. Res. Commun.* **473,** 469–473 (1996).

6. Hofmann, T. *et al.* Direct activation of human TRPC6 and TRPC3 channels by diacylglycerol. *Nature* **397,** 259–263 (1999).

7. Das, J. & Rahman, G. M. C1 Domains : Structure and Ligand-Binding Properties. *Chem. Rev.* **114,** 12108–12131 (2014).

8. Coussens, L. *et al.* Multiple, distinct forms of bovine and human protein kinase C suggest diversity in cellular signaling pathways. *Science* **233,** 859–866 (1986).

9. Rhee, J. S. *et al.* β phorbol ester- and diacylglycerol-induced augmentation of transmitter release is mediated by Munc13s and not by PKCs. *Cell* **108,** 121–133 (2002).

10. Wender, P. *et al.* Modeling of the bryostatins to the phorbol ester pharmacophore on

protein kinase C. *Proc. Natl. Acad. Sci. U. S. A.* **85,** 7197–7201 (1988).

11. Nadler, A. *et al.* The fatty acid composition of diacylglycerols determines local signaling patterns. *Angew. Chem. Int. Ed. Engl.* **52,** 6330–4 (2013).

12. Putyrski, M. & Schultz, C. Protein translocation as a tool: The current rapamycin story. *FEBS Lett.* **586,** 2097–2105 (2012).

13. Feng, S. *et al.* A rapidly reversible chemical dimerizer system to study lipid signaling in living cells. *Angew. Chemie - Int. Ed.* **53,** 6720–6723 (2014).

14. Toettcher, J. E., Voigt, C., Weiner, O. D. & Lim, W. The promise of optogenetics in cell biology: interrogating molecular circuits in space and time. *Nat. Methods* **8,** 35–38 (2012).

15. Frank, J. A. *et al.* Photoswitchable fatty acids enable optical control of TRPV1. *Nat. Commun.* **6,** 7118 (2015).

16. Davis, R. J., Ganongq, B. R., Belll, R. M. & Czech, M. P. 1,2-Dioctanoylglycerol. *J. Biol. Chem.* **260,** 1562–1566 (1985).

17. Oancea, E., Teruel, M. N., Quest, A. F. G. & Meyer, T. Green fluorescent protein (GFP)-tagged cysteine-rich domains from protein kinase C as fluorescent indicators for diacylglycerol signaling in living cells. *J. Cell Biol.* **140,** 485–498 (1998).

18. Wuttke, A., Idevall-Hagren, O. & Tengholm, A. P2Y1 receptor-dependent diacylglycerol signaling microdomains in beta cells promote insulin secretion. *FASEB J.* **27,** 1610–1620 (2013).

19. Nadler, A. *et al.* Exclusive photorelease of signalling lipids at the plasma membrane. *Nat. Commun.* **6,** 10056 (2015).

20. Zhao, Y. *et al.* An Expanded Palette of Genetically Encoded Ca2+ Indicators. *Science* **557,** 1888–1891 (2011).

21. Plenge-Tellechea, F. & Soler, F. On the inhibition mechanism of sarcoplasmic or endoplasmic reticulum Ca2+-ATPases by cyclopiazonic acid. *J. Biol. Chem.* **272,** 2794–2800 (1997).

22. Corbalán-García, S. & Gómez-Fernández, J. C. Protein kinase C regulatory domains: The art of decoding many different signals in membranes. *Biochim. Biophys. Acta - Mol. Cell Biol. Lipids* **1761,** 633–654 (2006).

23. Kikkawa, U., Matsuzaki, H. & Yamamoto, T. Protein kinase C delta (PKC delta): activation mechanisms and functions. *J. Biochem.* **132,** 831–839 (2002).

24. Reither, G., Schaefer, M. & Lipp, P. PKCalpha: A versatile key for decoding the cellular calcium toolkit. *J. Cell Biol.* **174,** 521–533 (2006).

25. Violin, J. D. & Newton, A. C. Pathway illuminated: visualizing protein kinase C signaling. *IUBMB Life* **55,** 653–660 (2003).

26. Violin, J. D., Zhang, J., Tsien, R. Y. & Newton, A. C. A genetically encoded fluorescent reporter reveals oscillatory phosphorylation by protein kinase C. *J. Cell Biol.* **161,** 899–909 (2003).

27. Toullecs, D. *et al.* The Bisindolemaleimide GF 109203X is a Potent and Selective Inhibitor of Protein Kinase C. *J. Biol. Chem.* **266,** 15771–15781 (1991).

28. Herbert, J. M., Augereau, J. M., Gleye, J. & Maffrand, J. P. Chelerythrine is a potent and specific inhibitor of protein kinase C. *Biochem. Biophys. Res. Commun.* **172,** 993–999 (1990).

29. Bergsten, P., Grapengiesser, E., Gylfe, E., Tengholm, A. & Hellman, B. Synchronous oscillations of cytoplasmic Ca2+ and insulin release in glucose-stimulated pancreatic islets. *J. Biol. Chem.* **269,** 8749–8753 (1994).

30. Yang, C. & Kazanietz, M. G. Divergence and complexities in DAG signaling: Looking beyond PKC. *Trends Pharmacol. Sci.* **24,** 602–608 (2003).

31. Kurohane Kaneko, Y. *et al.* Depression of Type I Diacylglycerol Kinases in Pancreatic β-Cells From Male Mice Results in Impaired Insulin Secretion. *Endocrinology* **154,** 4089–4098 (2013).

32. Ashcroft, F. M. *et al.* Stimulus-secretion coupling in pancreatic beta cells. *J Cell Biochem* **55S,** 54–65 (1994).

33. Jacobson, D. A. *et al.* Kv2.1 Ablation Alters Glucose-Induced Islet Electrical Activity, Enhancing Insulin Secretion. *Cell Metab.* **6,** 229–235 (2007).

34. Jacobson, D. A., Weber, C. R., Bao, S., Turk, J. & Philipson, L. H. Modulation of the Pancreatic Islet beta Cell delayed Rectifier Potassium Channel Kv2.1 by the Polyunsaturated Fatty arachidonate. *J. Biol. Chem.* **282,** 7442–7449 (2007).

35. Rutter, G. A. & Hodson, D. J. Beta cell connectivity in pancreatic islets: A type 2 diabetes target? *Cell. Mol. Life Sci.* **72,** 453–467 (2015).

36. Lou, X., Korogod, N., Brose, N. & Schneggenburger, R. Phorbol esters modulate spontaneous and Ca2+-evoked transmitter release via acting on both Munc13 and protein kinase C. *J. Neurosci.* **28,** 8257–8267 (2008).

37. Brose, N., Betz, A. & Wegmeyer, H. Divergent and convergent signaling by the diacylglycerol second messenger pathway in mammals. *Curr. Opin. Neurobiol.* **14,** 328–

340 (2004).

38. Basu, J., Betz, A., Brose, N. & Rosenmund, C. Munc13-1 C1 domain activation lowers the energy barrier for synaptic vesicle fusion. *J. Neurosci.* **27,** 1200–1210 (2007).

39. Wierda, K. D. B., Toonen, R. F. G., de Wit, H., Brussaard, A. B. & Verhage, M. Interdependence of PKC-Dependent and PKC-Independent Pathways for Presynaptic Plasticity. *Neuron* **54,** 275–290 (2007).

40. Betz, A. *et al.* Munc13-1 is a presynaptic phorbol ester receptor that enhances neurotransmitter release. *Neuron* **21,** 123–136 (1998).

41. Brose, N., Hofmann, K., Hata, Y. & Sudhof, T. C. Mammalian homologues of Caenorhabditis elegans unc-13 gene define novel family of C2-domain proteins. *J. Biol. Chem.* **270,** 25273–25280 (1995).

42. Varoqueaux, F. *et al.* Total arrest of spontaneous and evoked synaptic transmission but normal synaptogenesis in the absence of Munc13-mediated vesicle priming. *Proc. Natl. Acad. Sci. U. S. A.* **99,** 9037–42 (2002).

43. Bargmann, C. I. & Kaplan, J. M. Signal transduction in the Caenorhabditis elegans nervous system. *Annu. Rev. Neurosci.* **21,** 279–308 (1998).

44. Rand, J. B. Acetylcholine. *WormBook, ed C. elegans Res. Community* (2007). doi:/10.1895/wormbook.1.131.1.

45. Mahoney, T. R., Luo, S. & Nonet, M. L. Analysis of synaptic transmission in Caenorhabditis elegans using an aldicarb-sensitivity assay. *Nat. Protoc.* **1,** 1772–1777 (2006).

46. Fleming, J. T. *et al.* Caenorhabditis elegans levamisole resistance genes lev-1, unc-29, and unc-38 encode functional nicotinic acetylcholine receptor subunits. *J. Neurosci.* **17,** 5843–5857 (1997).

47. Lewis, J. a., Wu, C. H., Berg, H. & Levine, J. H. The genetics of levamisole resistance in the nematode Caenorhabditis elegans. *Genetics* **95,** 905–928 (1980).

48. Fliegl, H., Koehn, A., Haettig, C. & Ahlrichs, R. Ab Initio Calculation of the Vibrational and Electronic Spectra of trans- and cis-Azobenzene. *J. Am. Chem. Soc.* **125,** 9821–9827 (2003).

49. Nolan, C. J., Madiraju, M. S. R., Delghingaro-Augusto, V., Peyot, M.-L. & Prentki, M. Fatty Acid Signaling in the beta-Cell and Insulin Secretion. *Diabetes* **55,** S16–S23 (2006).

50. Konrad, D. B., Frank, J. A. & Trauner, D. Synthesis of Redshifted Azobenzene Photoswitches by Late-Stage Functionalization. *Chem. a Eur. J.* (2016).

ONLINE METHODS

Cell culture

HeLa Kyoto cells were grown in 1.0 g/L glucose Dulbecco's Modified Eagle Medium (DMEM, GIBCO, cat # 31885-023) supplied with 10% FBS (GIBCO, cat # 10270-106) and 0.1 mg/mL antibiotic Primocin (Invitrogen, cat # ant-pm-1). HeLa cells were first seeded in an 8-well Lab-Tek™ chambered coverslip (ThermoScientific # 155411) 24-48 h before transfection at 37 °C and 5% CO_2. Transfection was carried out with FugeneHD (Promega, cat # E2311) in DMEM free of FBS and antibiotic according to the manufacturer's instructions. First, the media was aspirated and the wells were charged with DMEM media (200 μL per well). A transfection solution containing DMEM (20 μL per well), cDNA (300 ng total DNA per well) and FugeneHD (1.5 μL per well) was then added to each well of the 8-well Lab-Tek™. Cells were incubated at 37 °C and 5% CO_2 for 20-24 h before the microscopy experiments were performed.

The mouse insulinoma derived cell line, MIN6, used in this study was initially developed and provided as a kind gift by Miyazaki *et al.*[51]. The cells were grown at 37 °C and 5% CO_2 in high glucose Dulbecco's Modified Eagle Medium (DMEM, 41965-039, Life Technologies) supplied with 15% Fetal Bovine Serum (FBS, 10270098, Lifetechnologies), penicillin-streptomycin (Pen Strep, 100 U/mL, 15140122, Lifetechnologies) and β-mercaptoethanol (70 μM, P07-05100, PAN-Biotech) that was always added freshly to the cell culture flasks. Cells were seeded in 8-well Lab-Tek™ microscope dishes 48–64 h (to reach 50-80% confluence) prior to imaging. For Ca^{2+} imaging, MIN6 cells were transfected with cDNA coding for the R-GECO[20] Ca^{2+} reporter, and cDNA coding for the C1-GFP[17] DAG sensor (as a control) usually 24–48 h after seeding. A transfection cocktail of C1-GFP (200 ng per well) and R-GECO (200 ng per well) in Opti-MEM (20 μL per well, 31985-070, Life Technologies) and Lipofectamine2000® transfection reagent (1.5 μL per well, 11668030, Life Technologies) was added to each well of an 8-well Lab-Tek™ microscope dish loaded with 200 μL Opti-MEM (37 °C, immediately before the addition). After

24 h incubation at 37 °C and 8.5% CO_2, the media was exchanged to culture media, followed by incubation for another 24 h before the microscopy experiments were performed.

Culture of primary mouse pancreatic islets

Islets were isolated from C57BL6 mice using collagenase digestion, as previously detailed[52]. Briefly, following euthanasia by cervical dislocation, the bile duct was injected with a collagenase solution (1 mg/mL) before digestion at 37 °C for 10 min and separation of islets using a Histopaque gradient (1.083 and 1.077 g/mL). Islets were cultured for 24–72 h in Roswell Park Memorial Institute (RPMI) medium supplemented with 10% fetal calf serum (FCS), 100 U/mL penicillin and 100 μg/mL streptomycin. Islets were dissociated into single β-cells using trypsin digestion for 5 min at 37 °C and allowed to attach to poly-L-lysine-coated and acid-etched coverslips. All animal work was regulated by the Home Office according to the Animals Act 1986 (Scientific Procedures) of the United Kingdom (PPL 70/7349, Dr Isabelle Leclerc), as well as EU Directive 2010/63/EU**.**

Laser scanning confocal microscopy

The cells were incubated in 250 μL imaging buffer containing (in mM): 115 NaCl, 1.2 $CaCl_2$, 1.2 $MgCl_2$, 1.2 K_2HPO_4, 20 HEPES, glucose (20 for MIN6, 11 for islets and β-cells unless otherwise stated), adjusted to pH 7.4 with NaOH at 37 °C and 5% CO_2 for at least 10 min. Compounds were first solubilized in DMSO at a concentration of 10 mM. This stock (2-5 μL) was then diluted into imaging buffer (50 μL) and added directly to the well containing the cells in imaging buffer.

Imaging of HeLa, MIN6, or primary rodent pancreatic β-cells was performed cells was performed on one of two microscopes: 1) Olympus Fluoview 1200 with a 20x objective, or a 63x oil objective. GFP excitation was performed with λ = 488 nm laser at low laser power (<3%) and emission was collected at λ = 500–550 nm. CFP excitation was performed with a λ = 405 nm laser at low laser power and emission was collected at λ = 425–475 nm. For FRET experiments, YFP emission was collected at λ = 510–560 nm. RFP/R-GECO excitation was performed with a λ = 559 nm laser at low laser power (<3%) and emission was collected at λ = 570-670 nm. Compound irradiation at λ = 375 nm was triggered using the quench function in the Olympus software. Photoactivation was carried out with λ = 375 nm laser at 100% intensity. 2) Zeiss Axiovert M200 coupled to a Yokogawa CSU10 spinning disk head and 10x and 20x objectives. Fluo-2 excitation was performed using a solid-state λ = 491 nm laser, and emission was collected using a highly sensitive back-illuminated EM-CCD (Hammamatsu C9100-13) at λ = 500–550 nm. Photoactivation was carried out using an X-Cite 120 epifluorescence source and a λ = 350±20 nm band-pass filter. Images were processed with Fiji software (http://fiji.sc/Fiji) and the resulting data was analyzed in Microsoft Excel, MATLAB and R. The data were then plotted with Igor Pro, Origin and R.

Quantification of insulin secretion

Insulin secretion was measured using static incubation of 6-8 islets for 30 min at 37 °C in Krebs-HEPES bicarbonate solution containing (in mM): 130 NaCl, 3.6 KCl, 1.5 $CaCl_2$, 0.5 $MgSO_4$, 0.5 NaH_2PO_4, 2 $NaHCO_3$, 10 HEPES and 0.1% (wt/vol) bovine serum albumin, pH 7.4[53]. Treatments were applied as indicated, and photoswitching performed at λ = 340±10 nm using a BMG Fluostar Optima platereader. Insulin concentration secreted into the supernatant was determined using a homogeneous time-resolved fluorescence (HTRF) assay (Cisbio), according to the manufacturer's instructions and low-range protocol.

Whole-cell electrophysiology in MIN6 and dissociated β-cells

MIN6 cells (passage 26–33) were cultured as described above at 37 °C and 5% CO_2. For cell detachment, the medium was removed and the cells were washed with Ca^{2+}-free PBS buffer and treated with trypsin for 5 min at 37 °C. The detached cells were diluted in growth medium and plated on acid-etched coverslips in a 24-well plate. 50,000 cells were added to each well in 500 μL growth medium. The growth medium was exchanged every 48 h, and electrophysiological experiments were carried out 2–7 days later.

Whole cell patch clamp experiments were performed using a standard electrophysiology setup equipped with a HEKA Patch Clamp EPC10 USB amplifier and PatchMaster software (HEKA Electronik). Micropipettes were generated from "Science Products GB200-F-8P with filament" pipettes using a Narishige PC-10 vertical puller. The patch pipette resistance varied between 4–7 MΩ. For recording of the Ca^{2+}-channel current[54], the bath solution contained (in mM): 82 NaCl, 20 tetraethylammonium chloride, 0.1 tolbutamide, 30 $CaCl_2$, 5 CsCl, 1 $MgCl_2$, 0.1 EGTA, 10 glucose, 5 HEPES (adjusted to pH 7.4 with NaOH). The intracellular solution contained (in mM): 102 CsCl, 10 tetraethylammonium chloride, 0.1 tolbutamide, 10 EGTA, 1 $MgCl_2$, 3 Na_2ATP, 5 HEPES (adjusted to pH 7.4 with CsOH). In voltage clamp mode, voltage steps were applied to the cells from the baseline at –70 mV to +50 mV in 10 mV intervals for 0.5 s. All cells had a leak current below 15 pA on break-in at –70 mV. For recording of the K_v current, the bath solution contained (in mM): 119 NaCl, 2 $CaCl_2$, 4.7 KCl, 10 HEPES, 1.2 $MgSO_4$, 1.2 KH_2PO_4, 14.4 glucose (adjusted to pH 7.3 with NaOH). The intracellular solution contained (in mM): 140 KCl, 1 $MgCl_2$, 10 EGTA, 10 HEPES, 5 MgATP (adjusted to pH 7.25 with KOH). The data was analyzed in Igor Pro using the Patcher`s Power Tools (MPI Göttingen) plugin. Current values were extrapolated and processed in Microscoft Excel, and the results were again plotted in Igor Pro.

Electrophysiology in mouse hippocampal neurons

Microisland cultures of wild type mouse hippocampal neurons were prepared as described[55]. For experiments, a 12-well plate was filled with 480 μL/well of extracellular recording solution contained (in mM): 140 NaCl, 2.4 KCl, 10 HEPES, 10 glucose, 4 $CaCl_2$, and 4 $MgCl_2$ (320 mOsmol/L), and 20 μL of a 12.5 M stock solution of **PhoDAG-2** or **PhoDAG-3** in DMSO was added. For controls, 20 μL of DMSO were added. The coverslips containing day *in vitro* 14–16 neurons were broken and a piece was moved into one well in the 12 well plate. The neurons were incubated at 37 ºC, and 5% CO_2 for 10 min with **PhoDAG-3** and respective controls; or for 20–25 min for **PhoDAG-2** and respective controls. Neurons were incubated with PhoDAG, and were whole-cell voltage clamped directly post-incubation. EPSCs were elicited by depolarization-induced action potentials at a frequency of 0.2 Hz. For vehicle controls, neurons from the same culture were incubated in DMSO for the same time. Beyond these times, we did not find a correlation between the length of incubation and the presence of an effect or its strength. Longer incubation periods of >1 h resulted in astrocyte death. In the case of **PhoDAG-2** patching the incubated neurons was usually easier 1 h after the stock solution was diluted in the extracellular solution. 3–4 coverslips were subsequently incubated in one well where either **PhoDAG-2** or **PhoDAG-3** were diluted.

Whole-cell voltage clamp recordings were acquired using the Axon Multiclamp 700B amplifier, Digidata 1440A data acquisition system, and the pCLAMP 10 software (Molecular Devices). The standard internal solution contained (in mM): 136 KCl, 17.8 HEPES, 1 EGTA, 4.6 $MgCl_2$, 4 NaATP, 0.3 Na_2GTP, 15 creatine phosphate, and 5 U/mL phosphocreatine kinase (315–320 mOsmol/liter), pH 7.4. Action potentials were stimulated at 0.2 Hz (by depolarizing the cell from –70 to 0 mV for 2 ms) to evoke excitatory post synaptic currents (EPSCs). The sEPSCs were derived from the traces where EPSCs were recorded (last 600 ms of a 1 s recording) and were recorded without tetrodotoxin (TTX). However, in the autapse-system, sEPSCs predominantly represent miniature EPSCs Light illumination was performed by a CoolLED pE-2 lamp that was fixed to the setup. Photoactivation was performed at λ = 365 nm (80% strength) and inactivation at λ = 425 nm (40% strength). The normalized responses following illumination were calculated by dividing by the averaged response before illumination. All analyses were performed using Axograph 1.4.3.

Aldicarb assay

Caenorhabditis elegans wild-type (N2) strain was cultivated at 20 °C on nematode growth medium (NGM) plates seeded with *E. coli* strain OP50-1[56]. A 100 mM stock solution of **PhoDAG-3** was prepared in 100% Ethanol. For application to *C.elegans,* the stock solution was diluted to the working concentration of 1 mM **PhoDAG-3** using OP50-1 and 200 μL of the resulting solution was applied to the NGM plate. For the vehicle control, an equivalent volume of 100% EtOH was used instead of the stock solution. L4 stage larvae were picked onto 1mM **PhoDAG-3**/EtOH NGM plates and left overnight. The young adult hermaphrodites were used on the following day for the aldicarb and levamisole-sensitivity assays[45,47]. The assay was performed in the dark, except for the picking and counting of animals which was performed under red light. To study aldicarb or levamisole sensitivity, 20 animals were transferred onto NGM plates containing 1 mM aldicarb (Sigma) or 0.1 mM tetramisole hydrochloride (Racemic form of levamisole, Sigma) and the fraction of animals paralysed was scored every 15 min by assessing movement following three gentle touches with a platinum wire. The animals were illuminated with UV-A light (366 nm, 18 $\mu W/mm^2$) provided by a UV-A lamp (Benda, Wiesloch, Germany) for the first 5 min after being placed on the aldicarb/levamsiole plates and then subsequently for the last 3 min of each 15 min time interval. The assays were performed blinded regarding the absence/presence of **PhoDAG-3**, and on the same day with the same batch of aldicarb or levamisole plates.

Data reporting and error analysis

For imaging experiments, “n” is the number of measurements made (individual cells). The number of independent experiments included in each panel is also described in the figure caption. For electrophysiological experiments, “n” represents the number of cells analyzed, each of which constitute an individual experiment. For insulin secretion experiments, “n” represents the number of independent experiments performed. For experiments in *C. elegans*, "n" represents the number of animals used, the number of experiments is also described in the figure caption. For all figure panels, results are plotted as mean ±s.e.m., using "n" as the number of samples. Where appropriate the Mann-Whitney test was used to determine statistical significance.

Synthetic protocols

All reagents and solvents were purchased from commercial sources (Sigma-Aldrich, TCI Europe N.V., Strem Chemicals, etc.) and were used without further purification unless otherwise noted. Tetrahydrofuran (THF) was distilled under a N_2 atmosphere from Na/benzophenone prior to use. Triethylamine (NEt_3), was distilled under a N_2 atmosphere from CaH_2 prior to use. Other dry solvents such as ethyl acetate (EtOAc), dichloromethane (CH_2Cl_2) and toluene (PhMe) were purchased from Acros Organics as "extra dry" reagents and used as received. Reactions were monitored by thin layer chromatography (TLC) on pre-coated, Merck Silica gel 60 F_{254} glass backed plates and the chromatograms were first visualized by UV-A irradiation at 254 nm, followed by staining with aqueous ninhydrin, anisaldehyde or ceric ammonium molybdate solution, and finally gentle heating with a heat gun. Flash silica gel chromatography was performed using silica gel (SiO_2, particle size 40–63 μm) purchased from Merck. Synthetic procedures are described in **Supplementary Notes 1-3**.

UV-Vis spectra were recorded using a Varian Cary 50 Bio UV-Visible Spectrophotometer with Helma SUPRASIL precision cuvettes (10 mm light path). All compounds were dissolved at a concentration of 25 μM in DMSO. Switching was achieved using a Polychrome V (Till Photonics) monochromator. The illumination was controlled using PolyCon3.1 software and the light was guided through a fiber-optic cable with the tip pointed directly into the top of the sample cuvette. An initial spectrum was recorded (*dark* adapted state, black) and then again following illumination at the λ_{max} for the π–π* transition (λ = 350 nm) for 3 min (*cis*-adapted state, purple). A third spectrum was recorded after irradiation at the λ_{max} for the n–π* transition (λ = 450 nm) for 3 min (*trans*-adapted state, blue).

All NMR spectra were measured on a BRUKER Avance III HD 400 equipped with a CryoProbe™. Multiplicities in the following experimental procedures are abbreviated as follows: s = singlet, d = doublet, t = triplet, q = quartet, quint = quintet, sext = sextet, hept = heptet, br = broad, m = multiplet. Proton chemical shifts are expressed in parts per million (ppm, δ scale) and are referenced to the residual protium in the NMR solvent ($CDCl_3$: δ = 7.26). Carbon chemical shifts are expressed in ppm (δ scale) and are referenced to the carbon resonance of the NMR solvent ($CDCl_3$: δ = 77.16). *NOTE: Due to the*

trans/cis equilibrium of some compounds containing an azobenzene functionality, more signals were observed in the ^{1}H and ^{13}C spectra than would be expected for the pure trans-isomer. Only signals for the major trans-isomer are reported, however the identities of the remaining peaks were verified by 2D COSY, HSQC and HMBC experiments. NMR spectra are displayed in **Supplementary Note 4**.

Infrared spectra (IR) were recorded as neat materials on a PERKIN ELMER Spectrum BX-59343 instrument. For detection a SMITHS DETECTION DuraSam-plIR II Diamond ATR sensor was used. The measured wave numbers are reported in cm^{-1}.

Low- and high-resolution EI mass spectra were obtained on a MAT CH7A mass spectrometer. Low- and high-resolution ESI mass spectra were obtained on a Varian MAT 711 MS instrument operating in either positive or negative ionization modes.

Methods References

51. Ishihara, H. *et al.* Pancreatic beta cell line MIN6 exhibits characteristics of glucose metabolism and glucose-stimulated insulin secretion similar to those of normal islets. *Diabetologia* **36,** 1139–1145 (1993).

52. Ravier, Magalie, A. & Rutter, Guy, A. in *Mouse Cell Cult.* **633,** 171–184 (2010).

53. Ravier, M. A. & Rutter, G. A. Glucose or Insulin, but not Zinc Ions, Inhibit Glucagon Secretion From Mouse Pancreatic alpha-cells. *Diabetes* **54,** 1789–1797 (2005).

54. Dadi, P. K. *et al.* Inhibition of Pancreatic beta-Cell Ca2+/Calmodulin-dependent Protein Kinase II Reduces Glucose-stimulated Calcium Influx and Insulin Secretion, Impairing Glucose Tolerance. *J. Biol. Chem.* **289,** 12435–12445 (2014).

55. Burgalossi, A. *et al.* Analysis of neurotransmitter release mechanisms by photolysis of caged Ca2+ in an autaptic neuron culture system. *Nat. Protoc.* **7,** 1351–1365 (2012).

56. Brenner, S. The genetics of Caenorhabditis elegans. *Genetics* **77,** 71–94 (1974).

COMPETING FINANCIAL INTERESTS

The authors declare no competing financial interests.